PCCP
Physical Chemistry Chemical Physics

Accepted Manuscript

This article can be cited before page numbers have been issued, to do this please use: M. L. Grasso, J. Puszkiel, L. Fernández Albanesi, M. Dornheim, C. Pistidda and F. C. Gennari, *Phys. Chem. Chem. Phys.*, 2019, DOI: 10.1039/C9CP03826D.

View Article Online
DOI: 10.1039/C9CP03826D

ARTICLE

CO_2 reutilization for methane production *via* catalytic process promoted by hydrides

Received 00th January 20xx,

Accepted 00th January 20xx

DOI: 10.1039/x0xx00000x

María L. Grasso[a], Julián Puszkiel [a,b], Luisa Fernández Albanesi[a], Martin Dornheim[b], Claudio Pistidda[b] and Fabiana C. Gennari[*a]

CO_2 emissions have been continuously increasing during the last half century with a relevant impact on the planet, being the main contributors of the greenhouse effect and global warming. The development of new technologies to mitigate these emissions poses a challenge. Herein, it is demonstrated the recycling of CO_2 to produce CH_4 selectively by using Mg_2FeH_6 and Mg_2NiH_4 complex hydrides as dual conversion promoters and hydrogen source. Magnesium based-metal hydrides containing Fe and Ni catalyze the hydrogenation of CO_2 and their total conversion is obtained at 400°C after 5 h and 10 h, respectively. The complete hydrogenation of CO_2 depends on the complex hydride, H_2:CO_2 mol ratio and experimental conditions: temperature and time. For both hydrides, the activation of CO_2 on the metal surface and its subsequent capture bring about the formation of MgO. Investigations on Mg_2FeH_6-CO_2 system indicate that the main process occurs via the reversed water-gas shift reaction (WGSR) followed by the methanation of CO in presence of steam. In contrast, the reduction of CO_2 by Mg-based hydride in the Mg_2NiH_4-CO_2 system has a strong contribution on the global process. Complex metal hydrides are promising dual promoter-hydrogen source for the CO_2 recycling and conversion into valuable fuels like CH_4.

1. Introduction

Two main linked phenomena threaten our nowadays social and environmental sustainability: depletion of conventional energy sources and global warming. Industries and means of transportation all over the world are based on fossil energy sources (carbon, petrol and gas). The intensified consumption of these conventional energy sources has been producing a rapid increase in CO_2 emissions, disrupting the global carbon cycle on the planet [1]. CO_2 concentration in the preindustrial era was around 280 ppm. However, it has already reached about 410 ppm, growing at a rate of 1% per year mainly due to anthropogenic activities [2,3]. This causes global warming and leads consequently to climate change, having detrimental ecological, physical and health impacts. In the last report of the Intergovernmental Panel on Climate Change (IPCC), it was shown that the annual greenhouse gases (GHG) emissions already reached a record of 53.5 $GtCO_2$ in 2017, being 0.7 $GtCO_2$ higher than in 2016. Based on these facts, global GHG emissions need to be reduced in 25% and 55% to limit the global temperature increase up to 2 °C and 1.5 °C, respectively[4].

To mitigate the negative effect of CO_2 on the planet, several approaches have been proposed and investigated. For example, the use of renewable energy sources, the application of CO_2 capture and storage (CCS) technologies and the transformation of CO_2 into value-added products have been proposed as the main plausible solutions[5-7]. Among them, the conversion of CO_2 is regarded as the most attractive technology since it constitutes the reuse of CO_2 waste for the catalytic production of synthetic fuels such as CH_4 and valuable chemicals like high alcohols. The methanation reaction, also known as Sabatier reaction[8,9], was first studied at the beginning of the last century. This reaction can be described by the following exothermic reaction:

$$CO_{2(g)} + 4H_{2\,(g)} \longrightarrow CH_{4\,(g)} + 2H_2O_{(g)} \quad (1)$$

The Sabatier reaction has been applied for the removal of carbon oxides in the feed gas for ammonia synthesis. Recently, this reaction gained renewed interest due to its potential application in power-to-gas technology [10,11]. The power-to-gas technology links the power grid with the gas grid by transforming all excess renewable energy into a grid compatible gas. As an example, hydrogen produced by water electrolysis can react with CO_2 released from power plants and then it can be transformed into methane. This synthetic gas can be stored and/or transported using

[a] Consejo Nacional de Investigaciones Científicas y Técnicas, CONICET - Instituto Balseiro (UNCuyo and CNEA). Departamento Fisicoquímica de Materiales, Gerencia de Investigación Aplicada, Centro Atómico Bariloche (CNEA), R8402AGP, S. C. de Bariloche, Río Negro, Argentina.
E-mail: gennari@cab.cnea.gov.ar, Phone: +54 294 4445118
[b] Department of Nanotechnology, Institute of Materials Research, Helmholtz-ZentrumGeesthacht, 21502, Geesthacht, Germany.
†Electronic Supplementary Information (ESI) available. See DOI: 10.1039/x0xx00000x

the existing gas distribution infrastructure, and/or it can be used in the well-established natural gas facilities.

Due to kinetic constraints of the reaction (1), the reduction of fully oxidized carbon to CH_4 requires the use of a catalyst to achieve fast rate and high selectivity. Currently, the methanation reaction operates between 200 °C and 550 °C [11,12], depending on the experimental conditions and the nature of the catalyst. The industrial application of the methanation process is nowadays restricted due to the lack of efficient and stable catalysts [13].

Different transition metals (TM) were investigated as active catalysts for CO_2 methanation. In these studies, it was found that the performance of a catalyst depends on the nature of the TM, the structures of clusters, catalyst´s support, etc. These properties have a clear effect on the adsorption, activation and reduction processes of CO_2. Chemisorption of CO_2 on transition metals is spontaneous. Moreover, the first metals in the 3d series present lower total barriers for CO_2 reduction [14]. Fe, Co, Ni and Cu metals have high catalytic properties for CO_2 activation. On the one hand, DFT calculations indicated that Fe prompts a thermodynamic sink on itself for CO_2. On the other hand, the interaction is energetically more favourable on Co and Ni for the involved elementary catalytic steps. Experimental tests showed that the CO_2 conversion at low temperature is a difficult process to carry out due to the high energy requirements [13,15]. Ni-based catalysts have been the most widely studied materials due to their high activity, high CH_4 selectivity and low cost. Despite these facts, Ni particles present some drawbacks such as deactivation due to sintering, coke deposition and toxicological concerns[15-17]. Co and Fe exhibit similar methanation activity as Ni. On the one hand, however, Co is not widely extended in industrial applications due to its high cost. On the other hand, Fe-based catalysts have reasonable activity, but their selectivity for CH_4 is usually low. Previous works [13-17] pointed out that transition metal particles play a key role on the CO_2 hydrogenation process; both in activation and reduction steps.

The nature of the catalyst´s support also has a determined effect on the microstructure and structure of the active phase, the adsorption step and the catalytic properties. The most common supports used in the industry are oxides, mixed oxides, zeolites, clays and mesoporous materials. Tada *et al.* studied the influence of different supports such as CeO_2, α-Al_2O_3, TiO_2 and MgO. They found that high conversion and selectivity were obtained for Ni/CeO_2 at low temperatures [16]. This was ascribed to the large adsorption of CO_2-derivative species promoted by the reduction of CeO_2 on the surface. However, it was shown that different supports have variable orders of basicity which favours the CO_2 adsorption and its activation. In the case of Ni/MgO catalyst, its higher activity was attributed to the basic properties of the MgO support on which CO_2 is strongly adsorbed [17]. Moreover, it was shown that MgO is able to initiate the methanation reaction by binding CO_2 at the surface forming magnesium carbonate species[18]. Supplying more hydrogen on this surface, further hydrogenation of magnesium carbonate to methane occurs. The addition of alkaline earth metals as promoters was also used to enhance the CO_2 activation and to increase the stability of hydrotalcite-derived catalysts[19-21]. For example, the effects of Fe and Mg as promoters for Ni-Al_2O_3-hydrotalcite was investigated. It was found that Ni dispersion is increased and the grain growth of NiO particles is also prevented [19].On the contrary, high Mg loading decreases the catalyst´s reducibility and therefore enhances the interaction of Ni with the support.

In search of new catalysts for the methanation reaction, hydrogen storage alloys are an attractive alternative to the classical catalysts used for CO_2 methanation. In 1990, Selvam *et al.* first reported the interactions between CO_2 and hydrogen storage alloys and compounds such as $LaNi_5$, $CaNi_5$, Mg_2Ni, Mg_2Cu, FeTiand Mg_2NiH_4 [22,23]. They observed the formation of carbonates on the surface as well as the usual formation of oxides and hydroxides. It was found that the oxidized surfaces with carbonate species on the top layers favour the reaction of these hydrogen storage materials with CO_2. In 2012, Kato *et al.*[24] investigated the changes on the surface of Mg_2NiH_4 during the dehydrogenation in CO_2 flow and studied the Mg_2NiH_4-CO_2 methanation reaction. These authors observed that the formation of surface oxide layers hinders the complete decomposition of the hydride phase. It was reported that the oxidation of the surface is related to the segregation of Mg oxides and Ni at the surface on Mg_2NiH_{4-x}. The precipitation of Ni-clusters at the surface ease the dissociation of H_2 and the modified surface becomes more active for CO_2 methanation. Hugelshofer *et al.*[25] showed that $LiAlH_4$ can react with CO_2, yielding CH_4, H_2 and metal oxides as main products at about 130 °C. Short-lived intermediate AlH_3 is formed in the presence of CO_2 and it acts as reducing agent, leading to CH_4 formation *via* formate and methoxy species.

In this work, the potential of Mg_2FeH_6 complex hydride for the conversion of CO_2 into CH_4 is explored for the first time under dynamic and static conditions. It was found that CO_2 hydrogenation to produce CH_4 is promoted by the presence of Fe, Ni and/or Mg-Ni alloys. The effect of the experimental conditions and the nature of the metal particles is also evaluated. This investigation provides a thermochemical method for CO_2 methanation using hydrogen provided from a portable storage material to selectively synthesize CH_4 under mild conditions. A combination of different techniques is applied in order to gain insights into the reaction mechanism.

2. Experimental

2.1 Thermodynamic calculations

The equilibrium compositions for H_2-CO_2 and Mg_2FeH_6-CO_2 systems as a function of the temperature were calculated using HSC Chemistry Windows, 6.1 version [26]. When all species in a reaction system are given (reactants and products), the software determines the distribution of the products where the Gibbs free energy of the system reaches its minimum at constant pressure. For the H_2-CO_2 system, the calculation was conducted based on gas phase containing H_2, O_2, CO, CO_2, CH_4, H_2O, C_2H_4, C_2H_6, CH_3OH and solid carbon, as possible species. For the equilibrium calculation of the 0.75Mg_2FeH_6-CO_2 system, the results were obtained for a reacting system composed of 4H_2-CO_2, with hydrogen provided from Mg_2FeH_6.

2.2 Materials preparation

MgH_2 (Rockwood, 99.8%), Fe (Alfa Aesar, 98%) and Ni (Alfa Aesar, 99%) were selected as starting materials. The complex metal hydrides, Mg_2FeH_6 and Mg_2NiH_4, were synthesized by a two-step procedure [27-29]. First, a mixture with 2:1 molar ratio of MgH_2 to metal (Fe or Ni, respectively) was hand mixed. Next, each mixture was mechanically milled under hydrogen atmosphere (10 bars of pressure) to improve the contact between particles and to hydrogenate all free Mg powders present in the Mg-based starting material [28]. The milling process was carried out in a planetary ball mill (Fritsch Pulverissete P6) for 5 hours using a ball to powder ratio of 10 to 1 and a rate of 500 rpm. All samples were handled in an Ar filled globe box to ensure their chemical stability. Figures S1A and S1B (curves a) show that the phases obtained after milling were MgH_2 and the free metal (Fe or Ni, respectively). The second step of the synthesis was a sintering process at high temperature (450°C) and high H_2 pressure (150 bars) for 5 hours. The XRPD (X-Ray Powder Diffraction) patterns obtained from the final products demonstrate the synthesis of Mg_2FeH_6 (cubic, S.G. Fm3m) and Mg_2NiH_4 (Monoclinic, S.G. C12/c1) as main phases (Figs. S1A and S1B, curves b). SEM photographs of Mg_2FeH_6 and Mg_2NiH_4 powders (Figs. S2A and S2B) show agglomerates of about 30 and 15 μm, respectively, with small particles rounded dispersed onto the surface. The element mapping results obtained by EDS indicate the homogeneous distribution of Mg and Fe or Ni elements.

2.3 Characterization techniques

The study of the reactivity of each hydride with CO_2 was done under flow and static conditions. Dynamic measurements were performed in a TGA analyzer (TG-HP50,TA Instruments) to follow mass change events and a Mass spectrometer (Hiden HPR-20 QIC)for a real time analysis of the gaseous products. In these experiments, the hydride sample was heated at 3 °C/min until 500 °C in a continuous flow of CO_2 (50 ml/min).

For the static measurements, it was employed a stainless steel reactor coupled to a Sieverts volumetric equipment, which allowed to select pressure and temperature conditions in the reactor. A specific mass of complex hydride sample was heated until 400°C (at 10°C/min) under a pressure of CO_2 to ensure a H_2:CO_2 ratio of 4:1. The hydride amount was estimated taking into account the hydrogen storage capacity of each hydride (Mg_2FeH_6 or Mg_2NiH_4). In each experiment, the gaseous products were analyzed by Fourier-Transform Infrared Spectroscopy (FTIR-Perkin Elmer Spectrum Series 400 Spectrometer) by collecting the gases released in a degassed quartz optical cell with KBr windows. The gas phase spectra were taken at room temperature and quantified using calibration curves.

Structural and morphological characterization of solid products were performed by solid-state FTIR, X-ray Powder Diffraction technique (XRPD, Bruker D8 Advance, using Cu-$K_\alpha$radiation) and Scanning Electron Microscopy (SEM-FIB, Zeiss, Crossbeam 340). The presence of carbon-based solids on the final products was analyzed by Raman spectroscopy with a confocal microscope (LabRAM HR Evolution Raman microscope)at room temperature and using the laser wavelength of 514 nm. For solid-state IR spectroscopy measurements, the powders were mixed with dry KBr under purified argon atmosphere, pressed to pellets and placed in a specially designed airtight cell.

3. Results and discussion

3.1 Interactions between CO_2-Mg_2NiH_4 and -Mg_2FeH_6 under dynamic conditions

As a first set of experiments, the dehydrogenation temperature of as-synthesized Mg_2FeH_6 and Mg_2NiH_4 was investigated using TG in He flow with a heating ramp of 3 °C/min (Figs. 1A and 1B, respectively, curves a).

The decomposition reaction of both Mg_2FeH_6 and Mg_2NiH_4 hydrides displays one-step dehydrogenation process. A hydrogen release of about 5.3 wt% is observed in the temperature range between 275 °C and 340 °C for Mg_2FeH_6, while ~3.5 wt% of hydrogen is quickly desorbed at 315 °C for Mg_2NiH_4.

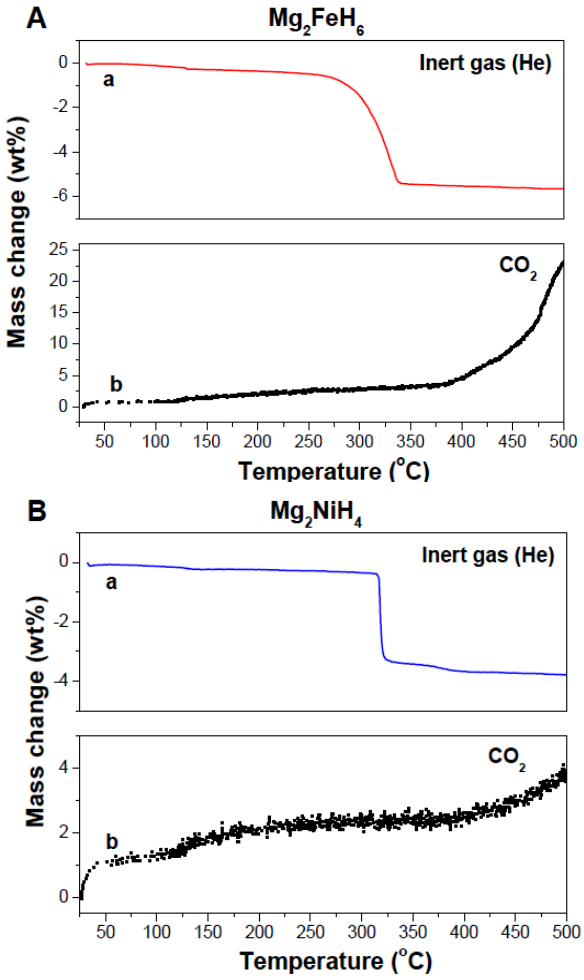

Fig. 1: TG curves of Mg_2FeH_6 (A) and Mg_2NiH_4 (B) heated in He (a) and CO_2 flow (b) up to 500 °C. Heating ramp: 3 °C/min; flow of 50 cm^3/min.

These hydrogen desorption amounts are in accordance with the theoretical ones of 5.4 wt% for Mg_2FeH_6 and 3.6 wt% for Mg_2NiH_4, respectively [27,30,31].

The characterization of the dehydrogenated samples at 500 °C (Fig. S3) by XRPD technique allows identifying Fe and Mg (or Mg_2Ni) as the main crystalline phases for Mg_2FeH_6(Mg_2NiH_4) decomposition[30-33]. Hence, decomposition of Mg_2FeH_6 and Mg_2NiH_4 under inert gas flow can be described by the following equations:

$$Mg_2FeH_{6\,(s)} \rightarrow 2\,Mg_{(s)} + Fe_{\,(s)} + 3\,H_{2(g)} \quad (2)$$

$$Mg_2NiH_{4\,(s)} \rightarrow Mg_2Ni_{\,(s)} + 2H_{2(g)} \quad (3)$$

in agreement with the literature[27,30].

In order to investigate the gas-solid reaction of CO_2 with Mg_2FeH_6 or Mg_2NiH_4 during heating, TG under CO_2 flow (Fig. 1) and simultaneous MS (Fig. 2) measurements were performed. Both hydrides only show mass gain (Figs.1A and 1B, curves b). For Mg_2FeH_6, a progressive CO_2 capture of 3.5 wt% is noticed up to 375 °C, followed by a sharp mass increase of 20 wt% between 375 °C and 500 °C (Fig. 1A). According MS analyses (Fig. 2A), two different reaction zones can be identified and are related with continuous hydrogen evolution between 375 °C and 525 °C. In the first zone, at about 405 °C, CO_2 conversion to CH_4 starts and the reaction extends for 45 min during Mg_2FeH_6 heating. In a second zone, the reaction with CO_2 occurs at 480 °C, providing more CH_4 as the major gaseous product, H_2 and minor amounts of CO. These two reaction zones are in good agreement with the mass gain rate observed in the TG curve between 375 °C and 500 °C (Fig. 1A). In the case of the interaction between CO_2 and Mg_2NiH_4, the TG curve shows ongoing mass increase of about 4.0 wt% from room temperature to 500 °C (Fig. 1B). The MS measurements (Fig. 2B) show one reaction zone between 365 °C and 410 °C, where the formation of minor amounts of CH_4 along with hydrogen are detected during 45 min. Additionally, CO is also observed within the detectable limit and its presence is also confirmed by gas FTIR.

Considering the mass increase of Mg_2FeH_6 and Mg_2NiH_4 during the heating under CO_2 flow, XRPD analyses of the solid samples after reaction were carried out (Fig. 3). The XRPD pattern of Mg_2FeH_6 heated up to 400 °C in CO_2 flow shows the presence of Fe and Mg (Fig. 3A), similar to the products formed during the Mg_2FeH_6 decomposition under inert atmosphere (reaction 2). Simultaneously, unreacted Mg_2FeH_6 remains, suggesting the incomplete Mg_2FeH_6-CO_2 reaction. After heating up to 500 °C (Fig. 3A), in addition to Mg and Fe phases, the formation of metal oxides: MgO and Fe_2O_3 are identified. Metal oxides might have also formed on the metal surfaces at lower temperatures. However, they are not detected by XRPD most likely due to their nanometric-layered structure.

Thus, the gas-solid reaction between Mg_2FeH_6 and CO_2 leads to the reduction of CO_2 to CH_4 and concomitantly the oxidation of Mg and Fe. In the case of Mg_2NiH_4, the phases identified after heating up to 400 °C in CO_2 flow are Ni, MgO and Mg_2Ni, while Mg_2NiH_4 remain unreacted (Fig. 3B). These phases correlate with the partial Mg_2NiH_4 decomposition (reaction 3) and partial disproportion of Mg_2Ni into Ni and Mg, which is then further oxidized. Heating up Mg_2NiH_4

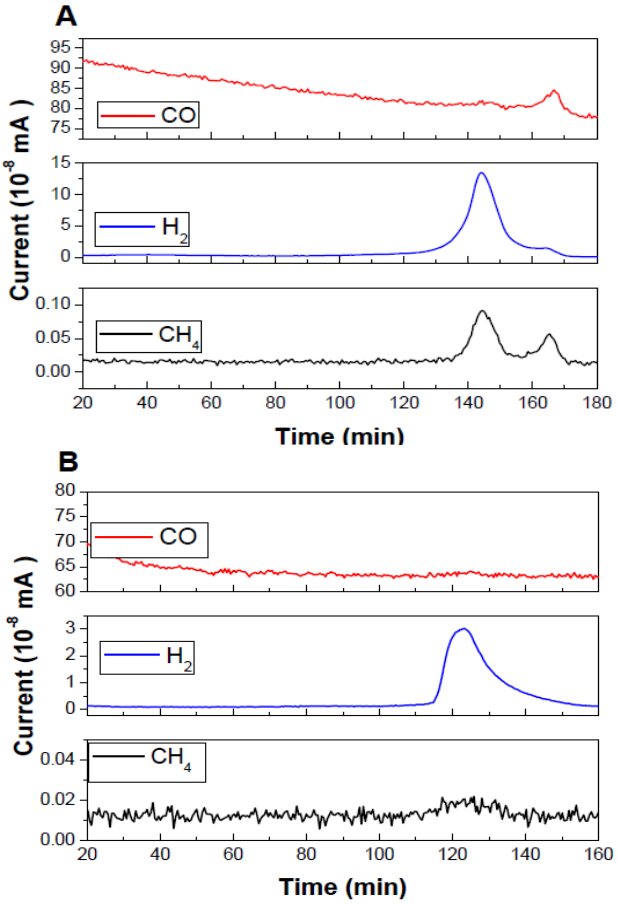

Fig. 2: MS of the gaseous species detected on heating of Mg_2FeH_6 (A) and Mg_2NiH_4 (B) in CO_2flow. Ramp: 3 °C/min; flow of 50 cm^3/min.

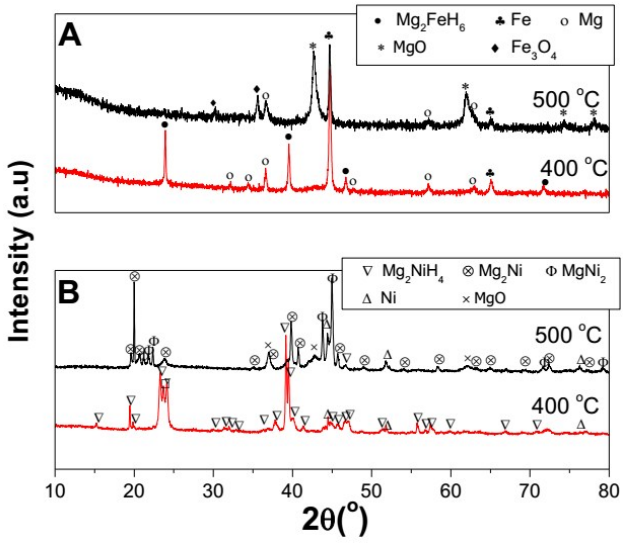

Fig. 3: XRPD patterns of Mg_2FeH_6 (A) and Mg_2NiH_4 (B) after heating in CO_2 flow. Ramp: 3 °C/min; flow of 50 cm^3/min.

View Article Online
DOI: 10.1039/C9CP03826D

under CO_2 to 500 °C results in its complete dehydrogenation and the further formation of MgO, simultaneously with Mg_2Ni, $MgNi_2$ and free Ni.

For both complex hydrides, it can be inferred that the mass gain accounts for an initial adsorption of CO_2 on the surface of the complex hydrides. This process delays the Mg_2FeH_6 and Mg_2NiH_4 dehydrogenation by passivation/oxidation of the surface (Fig. 1). This effect is more notable for the Mg-Fe-H system. As a consequence, hydrogen is released at higher temperature under CO_2 flow in comparison with the dehydrogenation under inert gas flow. In fact, as CO_2 is in contact with the hydride surface from room temperature, it might interact with the hydride by molecular adsorption or by dissociative chemisorption. In the case of an adsorption process, magnesium cations have large affinity for CO_2, forming oxides and in some case carbonates in the subsequent reaction steps[21].The dissociative chemisorption process, instead, involves the CO_2 splitting into CO(ads) and O(ads). Then, CO(ads) can be desorbed as CO(g) or react with H_2 released from the hydride phase and finally form CH_4. The O(ads) favours the surface oxidation and the segregation of MgO. It was reported, that disproportioned surfaces become more active in dissociating CO_2 and in promoting methanation[24]. As an evidence of these processes, XRPD analyses (Fig. 3) show the formation of MgO as well as the segregation of Ni or Fe and $MgNi_2$ coming from the interactions between both complex hydrides and CO_2. These phases formed *in situ* during hydride decomposition can act as catalysts for the methanation reaction [24,34].

3.2 Carbon dioxide transformation to methane by reaction with Mg_2NiH_4 and Mg_2FeH_6 under static conditions

To investigate the conversion of CO_2 in the presence of complex hydrides by heating in static conditions, FTIR analyses of the gaseous products were carried out. From the spectra displayed in Fig. 4, it can be noted that the thermal treatment of the Mg_2FeH_6 and Mg_2NiH_4 powders under CO_2 atmosphere (4:1 H_2:CO_2 mol ratio) at 400 °C for 1 h, 5 h and 10 h leads to the synthesis of CH_4 as main product. This is confirmed by the identification of the typical bands of CH_4 in the C-H bending region (1204-1390 cm^{-1}) and the C-H stretching modes (2818-3181 cm^{-1}). In addition, CO is detected after 1 h of heating simultaneously with unreacted CO_2 for both complex hydrides. Complete conversion of CO_2 to CH_4 is reached after 5 h for Mg_2FeH_6 at 400 °C, while in the case of Mg_2NiH_4, residual CO_2 and CO are also noted. It is known that CO chemisorption onto Ni particles retards the chemical process occurring on the Ni surface, such as the recombination of hydrogen[35]. Notably, no evidence of CO_2 bands is observed after heating both hydrides for 10 h, showing that CO_2 can be effectively transformed into CH_4.

Apparently, the conversion of CO_2 to CH_4 is enhanced by Mg_2FeH_6 in comparison with Mg_2NiH_4, indicating different kinetic behaviour and/or methanation mechanism for each hydride-CO_2 system. Furthermore, weak bands in the region of 3700 cm^{-1} and 1600 cm^{-1} are assigned to H_2O. No evidence of the formation of ethane, ethene, propane as well as methanol, all species detectable by FTIR spectrometer, are obtained. In this way, during the decomposition

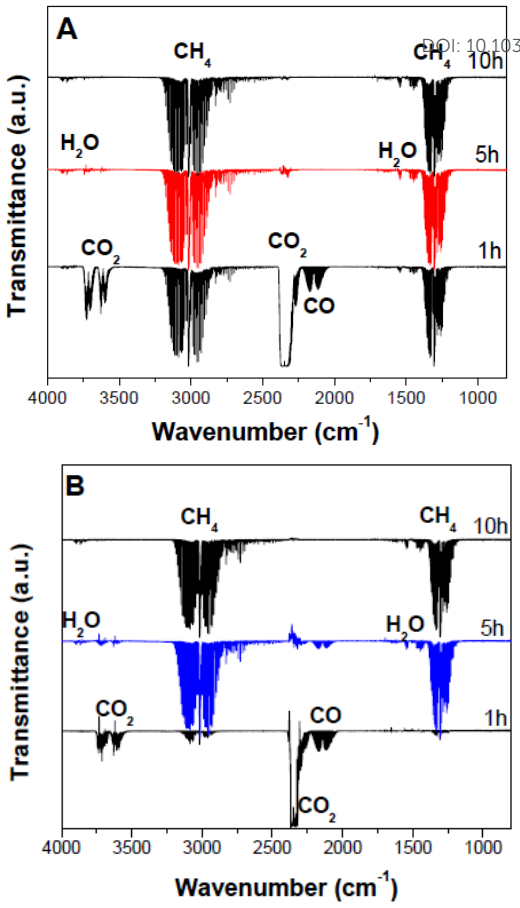

Fig. 4: FTIR spectra of the gas products for the reaction of: A) Mg_2FeH_6 and CO_2; B) $Mg_2NiH_4$and CO_2, at 400 °C for different times (H_2:CO_2= 4:1 mol ratio).

of the complex hydrides, CO and CH_4 are the only carbon containing products found in the gas phase. For comparison, Figure S4 shows the FTIR gas analysis after the reaction of complex hydrides with CO_2 using 2H_2:CO_2 mol ratio at 400 °C for 5 h. A decrease of the H_2:CO_2 mol ratio leads to the formation of CO and the detection of unreacted CO_2. Clearly, the conversion of CO_2 to CH_4 is strongly dependent on the starting H_2:CO_2 mol ratio.

To clarify the reaction mechanism between CO_2 and the complex hydrides, the structural changes of the solid products were investigated by XRPD. Figure 5 shows the XRPD patterns of the products formed after the reactions between Mg_2FeH_6 or Mg_2NiH_4 and CO_2 at 400 °C (Fig. 5A and 5B, respectively). In the case of Mg_2FeH_6-CO_2 system, after 1 h of reaction MgH_2, Fe and MgO phases are identified and Mg_2FeH_6 remain unreacted (Fig. 5A). Additional reaction time for 5 h induces the complete consumption of Mg_2FeH_6. The final phases after 5 h and 10 h are Fe, MgO, Mg and minor amount of MgH_2.

For the Mg_2NiH_4-CO_2 system, after 1 h of reaction MgH_2 and Ni are detected, indicating the partial Mg_2NiH_4 decomposition. At this time, partial oxidation of Mg to form MgO cannot be discarded but its presence is not detected probably due to its amorphous nature.

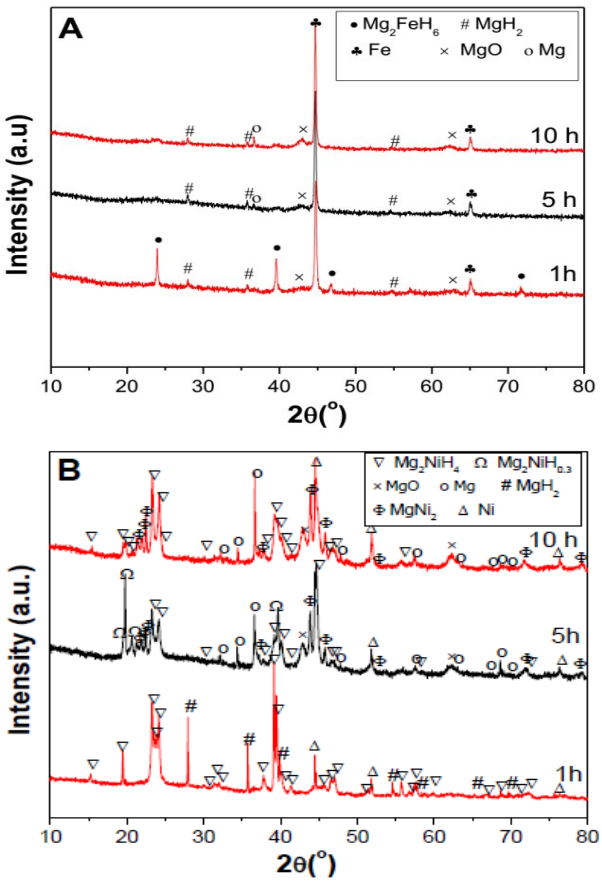

Fig. 5: XRPD patterns of the solid products after reaction between CO_2 and: A) Mg_2FeH_6; B) Mg_2NiH_4 at 400 °C for different times (H_2:CO_2= 4:1 mol ratio).

Additional reaction time for 5 and 10 h induces a progressive disproportion of Mg_2NiH_4 into $MgNi_2$, Ni and Mg, with simultaneous crystallization of MgO. The identification of MgH_2 and $MgNi_2$ during methanation by reaction of CO_2 with Mg_2FeH_6 and Mg_2NiH_4, respectively, point out that the disproportion of the surface is related with the reaction mechanism.

Morphological observations of the solid products obtained after 10 h of reaction between CO_2 with Mg_2FeH_6 or Mg_2NiH_4 at 400 °C are shown in Figures 6 and 7, respectively. SEM image in Fig. 6A shows a surface with micrometric agglomerate size with appreciable amount of pores. The surface is composed of faceted particles of MgO (Fig. 6B) surrounded by Fe spongy grains, as it was determined by EDS element mapping (Fig. S5). Figure 7A presents part of a Mg_2NiH_4 agglomerate composed of particles with spherical shape. EDS mapping of these spherical particles (Figs. 7B and S6) confirms their chemical nature as MgO. The MgO particles are wrapped around small Ni-containing particles. From these micrographs, it is also possible to observe that some spheres are hollow and have smooth surfaces. The vicinity of the MgO particles to the Fe or Ni particles suggests that the oxidation mechanism of Mg can be influenced by Fe or Ni as catalyst.

Mg_2FeH_6-CO_2 system displays superior results than Mg_2NiH_4-CO_2 regarding the conversion of CO_2. The obtained relative amount of CH_4 after 1 h at 400 °C is 30 times higher for Mg_2FeH_6-CO_2 system under the same static conditions ($4H_2$:CO_2 ratio), in agreement with the behaviour observed under dynamic conditions (Fig. 2).

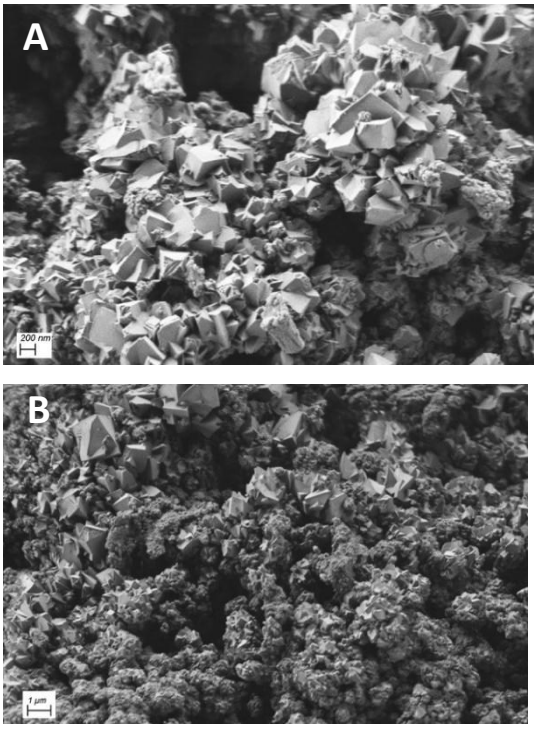

Fig. 6: SEM micrographs of the solid products after reaction between CO_2 and Mg_2FeH_6at 400 °C for 10 h: A) Surface of an agglomerate; B) Detail of the surface.

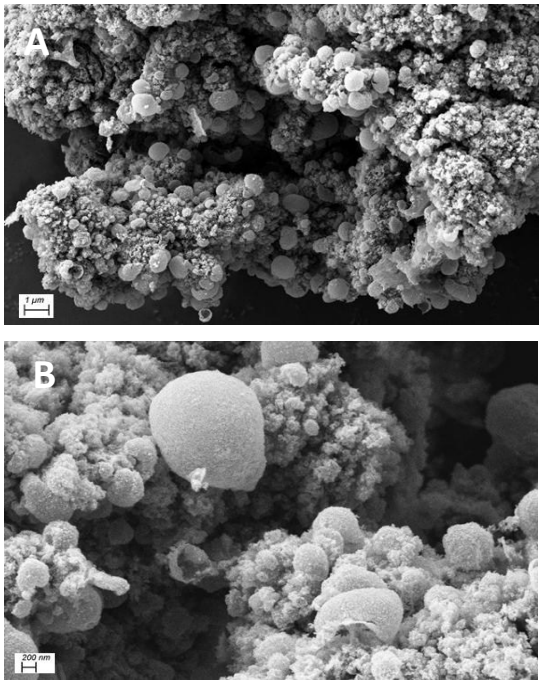

Fig. 7: SEM micrographs of the solid products after reaction between CO_2 and Mg_2NiH_4 at 400 °C for 10 h: A) Surface of an agglomerate; B) Detail of the surface.

View Article Online
DOI: 10.1039/C9CP03826D

In fact, complete CO_2 conversion is reached in 5 h at 400 °C and simultaneously Mg_2FeH_6 totally decomposes (Fig. 5).

In the case of Mg_2NiH_4, its partial decomposition after 1 h induces a limited production of CH_4 and CO. This result suggests that CO is chemisorbed on Ni poisoning both Ni/Mg-Ni catalytic surfaces[36]. As a consequence, dehydrogenation of Mg_2NiH_4 is retarded by hindering hydrogen recombination. At the same time, Mg is oxidized and the segregation of Ni and $MgNi_2$ occurs.

The Raman spectroscopic measurements of the residual solids after the reactions between the complex hydrides and CO_2 under dynamic (Fig. 8A) and static (Fig. 8B) conditions were conducted using the 514 nm laser. The Raman spectra for the Mg_2FeH_6-CO_2 system exhibit two strong peaks: the G mode at 1590 cm^{-1} originated from in-plane vibration of the sp^2 domain typical of graphite and the D mode at 1341 cm^{-1}, related to the defects and disorders in carbonaceous solid[37]. Moreover, after the reaction between Mg_2NiH_4 and CO_2, independently of the experimental conditions, any signal ascribed to G and/or D bands are detected. Therefore, the Raman analysis supports the formation of carbon during CH_4 production in the presence of Fe.

Solid-state FTIR studies on the sample obtained after methanation in static conditions for Mg_2NiH_4-CO_2 system provide additional information (Fig. 9). No relevant changes occur after 1 h of reaction, as it is confirmed by the identification of the band at 1630 cm^{-1} due to physisorbed water and a broad band around 3400 cm^{-1} due to surface hydroxyl groups. After 5 h of reaction, sharp vibration peaks of CH_x are identified and ascribed to the dissociation of CH_4 on the surface of Ni metal [38].

Additionally, in the region 1800-1200 cm^{-1} various bands are related with carbonate species. Among them, the bands at 1474 and 1385 $cm^{-1}$are attributed to unidentate carbonate, while the peak at 1630 cm^{-1}can be assigned to bicarbonate species [39]. The change in the intensities of these carbonates species indicates that there is a surface rearrangement of the sample during the methanation process in the presence of vapour water from 5 h to 10 h. Then,

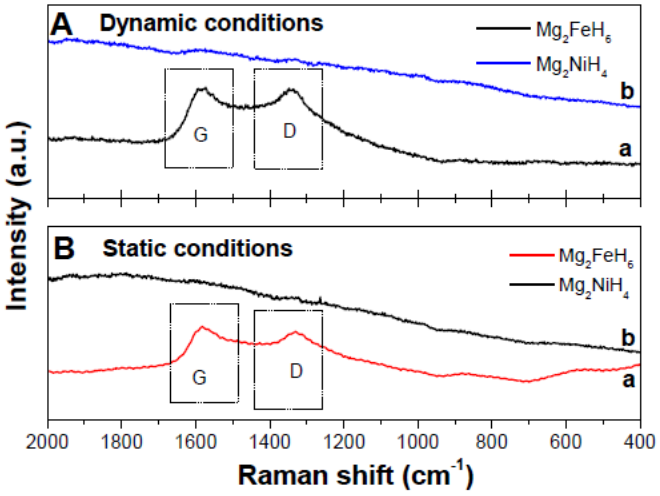

Fig. 8: Raman spectra of the (a) Mg_2FeH_6-$CO_2$and (b) Mg_2NiH_4-CO_2 systems after reaction under dynamic (A) and static conditions (B).

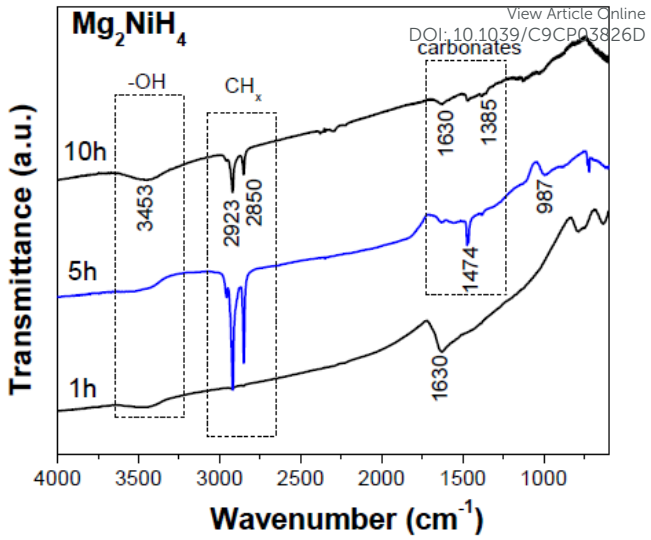

Fig. 9: Solid-state FTIR of the Mg_2NiH_4-CO_2 system after reaction under static conditions for different times.

during the methanation in presence of Ni based catalysts the formation of carbonates species instead of carbon is demonstrated.

3.3 Complex hydrides as alternative catalysts for methanation of CO_2

The methanation reaction is a complex process that depends on several factors such as temperature, pressure and composition of the reactants. An analysis of equilibrium composition by the Gibbs free energy minimization method is a useful tool to predict the distribution of products coming from multiple reactions in one system at chemical equilibrium. Gao *et al*. already analysed several of the above mentioned factors for the methanation reaction of CO_x[40]. In this work, by comparing thermodynamic calculations with experimental results, it is the aim to identify kinetic restrictions and specific interactions between the involved species. Therefore, it is possible to grasp the methanation mechanism involving solid hydrides.

Figure S7 shows the mol fraction of the products (%) as a function of temperature for CO_2 methanation at 1 bar and for $4H_2$:CO_2 molar ratio, calculated by Gibbs free energy minimization method [26]. From these calculations, it can be inferred that the optimal operating conditions for CO_2 methanation are relative low temperatures (up to 400 °C), where the CH_4 selectivity and CO_2 conversion are the highest. Despite the fact that it is expected that the reaction rate increases with the temperature, thermodynamic calculations indicate that above 450 °C the formation of CO by-product is favoured due to reversed water gas shift reaction. During the process, unreacted CO_2 and H_2 fractions also increase, while CH_4 product decrease.

In addition, no significant carbon deposition is predicted under the analyzed experimental conditions. It is also noted that when the H_2:CO_2 molar ratio decrease, CH_4 selectivity and CO_2 conversion strongly decrease as well, and thence carbon deposition is expected below 500 °C [40]. Thus, from the thermodynamic basis, to obtain high CH_4 yield and to avoid carbon deposition at 1 bar, both lower

temperatures than 400 °C and adequate H_2:CO_2 molar ratio higher than 4 are required for an optimized CO_2 methanation process.

The experimental results obtained under dynamic (Fig. 2) and static conditions (Fig. 4) show that the production of CH_4 is possible when CO_2 is in contact with the complex hydrides at about 400 °C. In these experiments, CH_4 is selectively produced and detected by MS and FTIR. Products such as ethane, propane or other hydrocarbon derivates are not observed during the experiments. The H_2:CO_2 ratio and the time of reaction between complex hydride-CO_2 at 400 °C, which is different under dynamic and static conditions, influence the performance of CH_4 production. Considering the experimental evidence, it can be proposed as a general statement that the methanation process takes place *via* the reversed water-gas shift reaction followed by the CO methanation in the presence of steam as follows:

$$CO_{2(g)} + H_{2(g)} \leftrightarrows CO_{(g)} + H_2O_{(g)} \quad (4)$$
$$CO_{(g)} + 3H_{2(g)} \leftrightarrows CH_{4(g)} + H_2O_{(g)} \quad (5)$$

These reactions are favoured by active catalytic species, such as Fe, Ni and/or Mg-Ni particles, which are formed during Mg_2FeH_6 and Mg_2NiH_4 decomposition (see Fig. 3) [13,14]. Indeed, during Mg_2FeH_6 and Mg_2NiH_4 heating up in CO_2 flow or in static CO_2 atmosphere, the formation of CO is detected as intermediate phase as well as CH_4 (Figs. 2 and 4). In the static experiment, CH_4 is observed simultaneously with minor amounts of steam (Fig. 4).

Thermodynamic calculations for the Mg_2FeH_6-CO_2 system with $4H_2$:CO_2 molar ratio and at 1 bar were performed to determine the equilibrium composition. It was not possible to extend the analysis for the Mg_2NiH_4-CO_2 system because of the lack of thermodynamic data of different Mg-Ni species. Figure 10 shows the evolution of the species as a function of temperature in equilibrium conditions for Mg_2FeH_6-CO_2 system. The thermodynamic calculations indicate that at 100 °C, Fe, MgH_2 and MgO are stable in the condensed phase, while CH_4 is practically the unique species in the gas phase. This result suggests that Mg_2FeH_6 partially decomposes at temperatures lower than 100 °C to produce CH_4 and Fe/Mg/MgH_2 as main solid phases.

Moreover, part of the MgH_2 reacts with CO_2 to produce MgO as follows:

$$2\,MgH_{2(s)} + CO_{2(g)} \leftrightarrows 2\,MgO_{(s)} + CH_{4(g)} \quad (6)$$

As the temperature increases, thermodynamic calculations predict two additional reactions, i.e. the decomposition of remnant MgH_2 and methane cracking:

$$MgH_{2(s)} \leftrightarrows Mg + H_{2(g)} \quad (7)$$
$$CH_{4(g)} \leftrightarrows C_{(s)} + 2\,H_{2(g)} \quad (8)$$

In contrast to the thermodynamic calculations, the experimental evidence demonstrates that Mg_2FeH_6 decomposition requires temperatures higher than 300 °C under He flow and about 375 °C under CO_2 flow (Fig. 1). This means that the dehydrogenation of

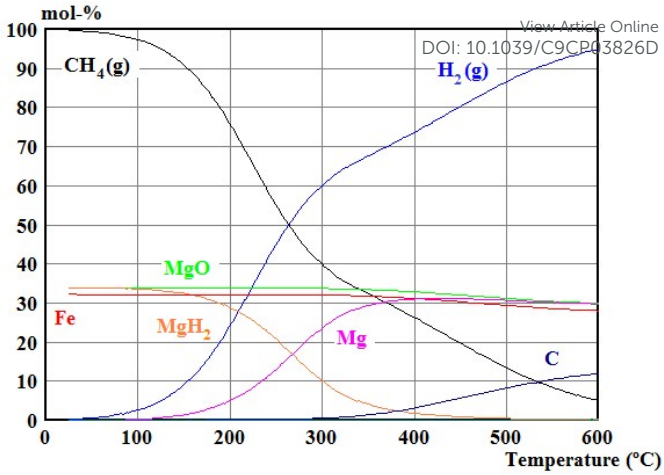

Fig.10: Equilibrium composition (mol%) as a function of temperature of the Mg_2FeH_6-CO_2system.

Mg_2FeH_6 is kinetically limited at temperatures lower than 300 °C, restricting the availability of hydrogen for the methanation of CO_2.

In the range of temperature between 350 °C and 450 °C, two contributions to the global process are possible. The main contribution is the methanation of CO_2 using Mg_2FeH_6 as hydrogen source (Fig. S7). In this case, it is possible to assume that the methanation takes place *via* the reversed water-gas shift reaction followed by the CO methanation in the presence of steam (reactions 4 and 5). These reactions are favoured by active catalytic species, such as Fe particles, which are formed during Mg_2FeH_6 decomposition and/or disproportion of the surface due to CO_2 activation. In accordance with the above proposed mechanism, during Mg_2FeH_6 heating under CO_2 flow or under static CO_2 atmosphere, the formation of CH_4 as well as CO as intermediate is verified (Figs. 2, 4 and S4). In fact, this mechanism is clarified by experiments done at 400 °C under different H_2:CO_2 ratios (Fig.4A and S3). With a $4H_2$:$1CO_2$ ratio, after 1 h the CO_2 conversion is partial and CO is detected, in accordance with reactions 4 and 5. However, after 5 h the total conversion of CO_2 is achieved. A $2H_2$:$1CO_2$ ratio leads to a partial conversion of CO_2, even after 5 h.

The other contribution to the global process is the formation of CH_4 *via* reaction (6), i.e. MgH_2 acting as reducing agent. However, this mechanism seems to have a minor contribution for the Mg_2FeH_6 and CO_2 interaction process. This is supported by the following observations: first, the CO formation is not predicted by the thermodynamic calculation as a product of the reduction of CO_2 by the hydride phase; second, a minor amount of MgO is detected; and third, the correlation between the total Mg_2FeH_6 decomposition (Fig. 5A) and consumption of CO_2 for the 4:1 molar ratio. Moreover, for the methanation reaction using Mg_2FeH_6 as hydrogen source, amorphous carbon is detected both under dynamic and static conditions (Fig. 8), probably promoted by the local ratio H_2:CO_2 <4 at 400 °C [40]. Carbon deposition can be originated from methane cracking (reaction 8). However, other possible reactions such as the Boudouart reaction, CO reduction or CO_2 reduction cannot be discarded [40].

The reaction pathway observed for the methanation of CO_2 using Mg_2FeH_6 is different from that reported for the thermochemical reduction of CO_2 promoted by alkali metal hydrides (LiH and NaH) [41] or alkaline earth metal hydrides [44] (MgH_2 and CaH_2). Indeed, Fe particles facilitates the methanation of CO_2 at 400 °C, leading to the partial conversion of CO_2 *via* CO formation after 1 h in presence of steam and reaching complete CO_2 conversion to CH_4 after 5 h for the H_2:CO_2 ratio of 4:1 (reactions 4 and 5).

The Mg_2NiH_4-CO_2 interaction at 400 °C presents a different mechanism. Although the catalytic methanation process (reactions 4 and 5) seems to operate at 400 °C, the experimental evidence after 10 h supports the fact that the reduction of CO_2 by Mg_2NiH_4 contributes to the global process: the complete decomposition of Mg_2NiH_4 is not reached, CO_2 is totally consumed and carbon deposition does not take place. This mechanism is partially associated with the poisoning of Ni-based compounds by CO after 1 h of reaction, hindering its further catalytic action. At the same time, CO_2 capture and disproportion of the surface occurs during Mg_2NiH_4 decomposition, with the formation of MgH_2, $MgNi_2$ and MgO. The carbonation of MgO leads to the formation of $MgCO_3$ on the surface after 5 h of reaction and posterior surface rearrangement in presence of water (Fig. 4B). Therefore, it is possible to propose that the methanation of CO_2 using Mg_2NiH_4 involves two simultaneous processes which are different in nature: the catalytic CO_2 conversion according to the reactions (4) and (5), and the direct reduction of CO_2 by the reducing effect of MgH_2 (reaction 6).

In two different investigations, the mechanochemical conversion of CO_2 to CH_4-H_2 gas mixture by lithium, magnesium and calcium hydrides was reported at room temperature and without any catalyst [42,43]. It was found that the mechanism of CO_2 reduction depends on the kind of metal hydride, the H_2:CO_2 ratio and the milling parameters. This process showed high selectivity to CH_4. However, the mechanochemical activation requires long times (24 h or 48 h) and the yield of CH_4 is low [42,43]. Recently, it was reported a CO_2 thermochemical reduction process to produce CH_4 and H_2 fuels using ball milled alkali metal hydrides (LiH or NaH) [41] or alkaline-earth metal hydrides (CaH_2 and MgH_2) [44]. The first study with alkali metal hydrides showed that the yield of CH_4 depends on the reaction time and temperature at 4:1 H_2:CO_2 mol ratio. [41] The optimal performance was obtained at 450 °C within 48 h for both CO_2-LiH and CO_2-NaH reaction systems. Similarly, the performance of the CaH_2 and MgH_2 also showed a strong dependence on the reaction time, temperature and H_2:CO_2 mol ratio. Our investigation provides a clear contribution to the already published investigations where CO_2 conversion to CH_4 is performed by mechanochemical activated process of LiH/CaH_2/MgH_2 or thermochemical process of mechanical activated LiH/NaH/MgH_2/CaH_2 without catalyst. In these works, the authors reported that the reduction of CO_2 without catalyst is highly efficient, and selective. Though, in comparison with this work, these processes require both higher temperature (450 °C) and longer times (48 h). Here, the total conversion of CO_2 is obtained using as-synthesized Mg_2FeH_6 complex hydride, a Mg based hydride without mechanical activation, as a portable storage material to selectively prepare CH_4 at 400 °C in 5 h. Optimization of the reaction conditions using portable Mg-based hydrides with different catalyst is still subject of current investigations.

4. Conclusions

In this work, we demonstrate for the first time, to the best of our knowledge, that Mg_2FeH_6 can be used as hydrogen source to selectively convert CO_2 into CH_4 under controlled experimental conditions. It was found that the total conversion of CO_2 is reached after 5 h of heating at 400 °C with a 4H_2:CO_2 molar ratio by catalytic action of Fe particles. The global mechanism involves the reversed water-gas shift reaction followed by methanation of CO in presence of steam. After 10 h of reaction, partial oxidation of Mg and carbon deposition is observed. Investigations on the methanation mechanism of CO_2 *via* Mg_2NiH_4 indicates that the direct reduction of CO_2 caused by the MgH_2/Mg_2NiH_4 hydride system plays an important role on the whole process. Carbonation of MgO is confirmed after 5 h of reaction.

This investigation provides a thermochemical method to capture and selectively synthesize CH_4. This method involves the dual utilization of low-cost and portable metal hydride phases, i.e. Mg_2FeH_6 and Mg_2NiH_4. On the one hand, complex hydrides act as hydrogen sources. On the other hand, these complex hydrides provide catalytic species with high selectivity, promoting the full conversion of CO_2 into CH_4. The high selectivity of the reaction is actually a determined factor for the application of CO_2–CH_4 conversion technologies. As a matter of fact, CH_4 has the highest hydrogen/carbon ratio among all hydrocarbons and it also has the largest heat of combustion in comparison with the gasoline. The utilization of CH_4 presents a big advantage since the infrastructure necessary for domestic and industrial use is already available. Therefore, it is here proposed an efficient process for *in situ* CO_2 recycling and conversion into CH_4, avoiding CH_4 storage and/or transport.

Conflicts of interest

There are no conflicts to declare

Acknowledgements

The present work is part of the CO2MPRISE, "CO_2 absorbing Materials Project- RISE", a project that has received funding from the European Union's Horizon 2020 research and innovation programme, under the Marie Skłodowska-Curie Grant Agreement No 734873. The work was also supported by CONICET (Consejo Nacional de Investigaciones Científicas y Técnicas), ANPCyT– (Agencia Nacional de Promoción Científica y Tecnológica), CNEA (Comisión Nacional de Energía Atómica) and HZG (Helmholtz–ZentrumGeesthacht). The authors also thank Bernardo Pentke (Departamento Fisicoquímica de Materiales) for the SEM

micrographs and Sebastian Anguiano for the Raman measurements (Laboratorio de Fotónica y fotoelectrónica).

Notes and references

1 D. A. J. Rand and R. M. Dell, *RSC Publishing*,2008, 7-32.
2 D. Lüthi, M. Le Floch, B. Bereiter, T. Blunier, J-M. Barnola, U. Siegenthaler, D. Raynaud, J. Jouzel, H. Fischer, K. Kawamura, T.F.Stocker, *Nature,*2008, **453**, 379-382.
3 K. Schaefer, H.Lantuit, V.E.Romanovsky, E.A.G. Schuur, R.Witt, *Environ. Res.Lett.*2014, **9**, 1-9.
4 A.Olhoff, *IPCC Side Event COP*, 2018, **24**, 1-19.
5 D. Leung, G. Caramanna, M.Maroto-Valer, *Renew. Sust. Eneg. Rev,* 2014, **39**, 426-443.
6 M. Bui, C. Adjiman, A. Bardow, E. Anthony, A. Boston, S. Brown, P. Fennell, *Energy Environ.Sci.*2018, **11**, 1062-1176.
7 M. Aresta, A. Dibenedetto, A. Angelini, *Chem. Rev.* 2014, **114**, 1709-1742.
8 P. Sabatier, J.B. Senderens, *Acad. Sci. Paris,*1902, **134**, 514-516.
9 M.A. Vannice, *Springer*, 1982, 139-198.
10 M. Götz, J. Lefebvre, F. Mörs, A.M.D. Koch, F. Graf, S. Bajohr, R. Reimert,T. Kolb, *Renew. Energy,*2016,**85**, 1371-1390.
11 T. Schaaf, J. Grünig, M. Roman Schuster, T. Rothenfluh, A. Orth, *Energy Sustain Soc.*,2014, **4 (1)**, 2–14.
12 S. Rönsch, J. Schneider, S.Matthischke, M. Schlüter, M. Götz, J. Lefebvre, P. Prabhakaran, S. Bajohr, *Fuel,* 2016, **166**, 276–296.
13 M. Younas, L.L. Kong, M.J.K. Bashir, H. Nadeem, A. Shehzad, S. Sethupathi, *Energy Fuels,* 2016, **30**, 8815-8831.
14 C. Lui; T. R. Cundari; A. K. Wilson, CO_2 reduction on Transition Metal (Fe, Co, Ni and Cu) surfaces: In comparison with Heterogeneous Catalysis. *J Phys. Chem. C,* 2012, **116**, 5681-5688.
15 S. De, J. Zhang, R. Luque, N. Yan, *Energy Environ. Sci.*,2016, **9**, 3314-3347
16 S. Tada, T. Shimizu, H. Kameyama, T. Haneda, R. Kikuchi, *Int. J. Hydrogen Energy*, 2012, **37**, 5527-5531.
17 M. Guo, G.Lu, *Catal. Commun*. 2014, **54**, 55–60.
18 J.N. Park, E.W.A. McFarland, *J. Catal.,*2009, **266,** 92–97.
19 X. Wang, T. Zhen, C. Yu, *Appl. Petrochem Res.,* 2016, **6(15)**,1–7.
20 J. Shen, J.M. Kobe, Y. Chen, J.A. Dumesic, J.A.,*Langmuir,*1994, **10(10)**,3902-3908.
21 D. Wierzbicki, R. Debeka, M. Motak, T. Grzybek, M.E. Gálvez, P. Da Costa, *Catal.Commun*. 2016, **83**,5-8.
22 P. Selvam, B. Viswanathan, V. Srinivasan, *J Less Common Met*., 1990, **158**, L1-L7.
23 P. Selvam, B. Viswanathan, V. Srinivasan, V. *Int J Hydrogen Energy*,1990, **15** (2), 133-137.
24 K. Kato, K.; A. Borgschulte, D. Ferri, M. Bielmann, J-C. Crivello, D. Wiedenmann, M. Parlinska-Wojtan, P. Rossbach, Y. Lu, A. Remhofa, A. Zuttel, *Phys. Chem. Chem. Phys*., 2012, **14**, 5518–5526.
25 C.L. Hugelshofer, A. Borgschulte, E. Callini, S.K. Matam, J. Gehrig, D. Hog, A. Züttel,*J PhysChem C,* 2014, **118**, 15940−15945.
26 H.S.C. Outokumpu, Chemistry For Windows, Version 6.1, Outokumpu Research Oy, Finland, 2009.
27 M. Polanski, T.K. Nielsen, Y. Cerenius, J. Kunce, J.Bystrzycki,*Int. J. Hydrogen Energy,* 2010, **35 (8)**, 3778-3782.
28 P. Selvam, K. Yvon, *Int. J. Hydrogen Energy,* 1991, **16**, 615-617.
29 J. C. Bobet, E. Akiba, Y. Nakamura, B. Darriet, *Int. J. Hydrogen Energy,* 2000, **25(10)**, 987-996.
30 J. A Puszkiel, J.J Andrade-Gamboa, F.C. Gennari, *K. Y. Cheong, G. Impellizzeri, M. Fraga Editors*, 2018, 394-424.
31 M. Polanski, T.K. Nielsen, I. Kunce, M.Norek, T.Płociński, C.; Jaroszew Gundlach, T.R. Jensen, *Int. J. Hydrogen Energy,*2013,**38**, 4003-4010.
32 F.C. Gennari, F.J. Castro, J.J. Andrade Gamboa, J. *J. Alloys Compd.,* 2002, **339**, 261-267.
33 J. A. Puszkiel, F.C. Gennari, P. Arneodo Larochette, F. Karimi, C. Pistidda, R. Gosalawit-Utke, J. Jepsen, T. Jensen, C. Gundlach, J. Bellosta von Colbe, T. Klassen, M. Dornheim, *Int. J. Hydrogen Energy,* 2013, **38**, 14618-14630.
34 G. Mulas, R. Campesi, S. Garroni, F.Delogu, C. Milanese, *Appl. Surface Sci*.,2011, **257**, 8165-8170.
35 W,N. Shen, J.A. Dumesic, *J. Catal.,* 1981, **68**, 152-165.
36 E. Fromm, *Springer- Verlag*, 1998.
37 J. Hong, M.K. Park, E.J., D. E. Lee, D. S. Hwang, S. Ryu, *Scientific Reports,* 2013, **3**, 2700.
38 G. Jianzhong, H. Zhaoyin, G.Jing, Z. Xiaoming, *Chinise J. Catalysis,*2007, **28**, 22-26.
39 H. Du, C.T. Williams, A.D. Ebner, J.A. Ritter, *Chem. Mater,* 2010, **22**, 3519-26.
40 J. Gao, Y. Wang, Y. Ping, D. Hu, G. Xu. F. Gu, F. Su, *RSC Adv*., 2012, **2**, 2358–2368.
41 B-X. Dong, L-Z. Wang, L. Song, J. Zhao, Y-L. Teng, *Energy Fuels,* 2016, **30**, 6620-6625.
42 B.-X. Dong, J. Zhao, L.-Z. Wang, Y.-L. Teng, W.-L. Liu, L. Wang, *Appl. Energy,*2017, **204**, 741-748.
43 K. Pu, Y. Yang, X. Qu, M. Gao, B-X. Dong, Y. Liu, H. Pan, *Chem. Select,*2017, **2**, 5244-5247.
44 J. Zhao, Y-F. Wei, Y-L. Cai, L-Z. Wang, J. Xie, Y-L. Teng, W.Zhu, M. Shen, B-X. Dong, *ACS Sustainable Chem. Eng.,* 2019, **7**, 4831-4841.

View Article Online
DOI: 10.1039/C9CP03826D

ABSTRACT GRAPHICS

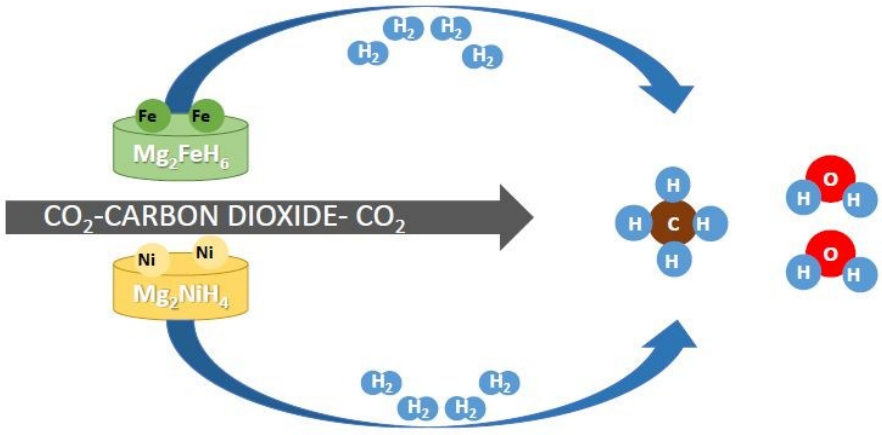

CO_2 is recycled to produce CH_4 selectively by using complex hydrides as hydrogen source and catalytic metal particles.